the plant journal

SEB SOCIETY FOR EXPERIMENTAL BIOLOGY

The Plant Journal (2022) **109,** 261–277 doi: 10.1111/tpj.15555

RESOURCE

Dynamic light- and acetate-dependent regulation of the proteome and lysine acetylome of *Chlamydomonas*

Magdalena Füßl[1,2,3,†], Ann-Christine König[1,2,4,†], Jürgen Eirich[3], Markus Hartl[1,2,5], Laura Kleinknecht[2], Alexandra-Viola Bohne[2], Anne Harzen[1], Katharina Kramer[1], Dario Leister[2], Jörg Nickelsen[2] and Iris Finkemeier[1,2,3,*]

[1]*Plant Proteomics, Max Planck Institute for Plant Breeding Research, Carl von Linné Weg 10, Cologne DE-50829, Germany,*
[2]*Faculty of Biology, Ludwig-Maximilians-University, Grosshaderner Strasse 2-4, Munich DE-82152, Germany,*
[3]*Plant Physiology, Institute of Plant Biology and Biotechnology, University of Muenster, Schlossplatz 7, Muenster DE-48149, Germany,*
[4]*Helmholtz Zentrum München, German Research Center for Environmental Health, Research Unit Protein Science, Heidemannstr. 1, Munich DE-80939, Germany, and*
[5]*Mass Spectrometry Facility, Max Perutz Labs, University of Vienna, Vienna Biocenter (VBC), Dr. Bohr-Gasse 7, Vienna AT-1030, Austria*

Received 26 July 2021; revised 19 October 2021; accepted 22 October 2021; published online 28 October 2021.
*For correspondence (e-mail iris.finkemeier@uni-muenster.de).
[†]These authors contributed equally to this work.

SUMMARY

The green alga *Chlamydomonas reinhardtii* is one of the most studied microorganisms in photosynthesis research and for biofuel production. A detailed understanding of the dynamic regulation of its carbon metabolism is therefore crucial for metabolic engineering. Post-translational modifications can act as molecular switches for the control of protein function. Acetylation of the ε-amino group of lysine residues is a dynamic modification on proteins across organisms from all kingdoms. Here, we performed mass spectrometry-based profiling of proteome and lysine acetylome dynamics in *Chlamydomonas* under varying growth conditions. *Chlamydomonas* liquid cultures were transferred from mixotrophic (light and acetate as carbon source) to heterotrophic (dark and acetate) or photoautotrophic (light only) growth conditions for 30 h before harvest. In total, 5863 protein groups and 1376 lysine acetylation sites were identified with a false discovery rate of <1%. As a major result of this study, our data show that dynamic changes in the abundance of lysine acetylation on various enzymes involved in photosynthesis, fatty acid metabolism, and the glyoxylate cycle are dependent on acetate and light. Exemplary determination of acetylation site stoichiometries revealed particularly high occupancy levels on K175 of the large subunit of RuBisCO and K99 and K340 of peroxisomal citrate synthase under heterotrophic conditions. The lysine acetylation stoichiometries correlated with increased activities of cellular citrate synthase and the known inactivation of the Calvin–Benson cycle under heterotrophic conditions. In conclusion, the newly identified dynamic lysine acetylation sites may be of great value for genetic engineering of metabolic pathways in *Chlamydomonas*.

Keywords: *Chlamydomonas*, lysine acetylation, acetate, proteome, citrate synthase, glyoxylate cycle, RuBisCO.

INTRODUCTION

The soil-dwelling green alga *Chlamydomonas reinhardtii* (hereafter *Chlamydomonas*) is one of the most studied microorganisms in photosynthesis research and for biofuel production, because of its ability to use different carbon sources for its growth (Leite et al., 2013; Merchant et al., 2012). *Chlamydomonas* can grow photoautotrophically with just light as an energy source for carbon dioxide fixation, as well as heterotrophically with acetate as carbon source for respiration. In addition, *Chlamydomonas* is often grown in a mixture between both conditions (acetate and light), which is named mixotrophic growth (Hoober, 1989). Using chloroplastic and nuclear genome engineering, enhancing *Chlamydomonas* characteristics for biofuel production has

been achieved over the last years (Scranton et al., 2015). Still there is a huge gap of knowledge about the underlying biochemistry and regulation of metabolic processes in *Chlamydomonas*. Hence, to further develop the usage of *Chlamydomonas* as an alternative source for biofuel production, the main challenge is to understand the regulatory mechanisms of its metabolic pathways. Metabolic flux balance analyses have revealed the different metabolic pathways that *Chlamydomonas* uses depending on different growth conditions (Boyle and Morgan, 2009). However, the underlying mechanisms which enable fast regulation of protein activity under variable growth conditions are still not fully uncovered. An acclimation to growth conditions can occur on several levels, which include transcriptional and translational control, as well as protein stability, product inhibition, and allosteric effects on enzyme activities (Erickson et al., 2015; Hoober, 1989; Ledford et al., 2007). The effects of acetate on photosynthesis, gene expression, and metabolite pools have already been largely established in *Chlamydomonas* and other green algae (Bogaert et al., 2019; Boyle and Morgan, 2009; Boyle et al., 2017; Hayashi et al., 2015; Lauersen et al., 2016; Rai et al., 2013; Roach et al., 2013; Smith et al., 2015). To utilize C_2 compounds, such as acetate, *Chlamydomonas* uses the glyoxylate cycle to form C_4 compounds, which can be further metabolized to amino acids or soluble carbohydrates (Lauersen et al., 2016). Five out of six enzymes associated with the glyoxylate cycle are localized in the peroxisomal microbodies. Peroxisomes in algae are referred to as peroxisomal microbodies since they contain fewer proteins than those in higher plants (Kato et al., 1997; Stabenau, 1974; Stabenau et al., 1993).

Another mechanism for a fast metabolic acclimation to acetate-containing medium might be mediated by post-translational protein modifications (PTMs) (Kaur et al., 2021). Such modifications can act as reversible molecular switches, which enable proteins to change their activities, functions, or even localizations in the cell (Castano-Cerezo et al., 2014; Jing et al., 2013). Nearly nothing is known about PTM-dependent regulation of metabolic pathways in *Chlamydomonas*. Next to protein phosphorylation, lysine acetylation (acK) is one of the most prominent PTMs and occurs on the ε-amino group of the lysine side chain. In eukaryotes, lysine acetylation was discovered in the context of histones and gene expression, where it is linked to transcriptional regulation by changing the interaction of transcription factors with the chromatin (Sterner and Berger, 2000). In *Chlamydomonas*, alpha-tubulin in axonemal microtubules was discovered as the first non-nuclear lysine-acetylated protein more than 30 years ago (L'Hernault and Rosenbaum, 1983, 1985). Lysine acetylation is nowadays known to occur in all kingdoms of life on proteins from various subcellular localizations, and is particularly important for the regulation of metabolism, as well as photosynthesis in plants (Finkemeier et al., 2011; Hartl et al., 2017; Hosp et al., 2017; Koskela et al., 2020; Liu et al., 2021; Narita et al., 2019; Wu et al., 2011). Recently, it was shown that lysine acetylation is directly connected to acetate metabolism in *Escherichia coli* (Weinert et al., 2017). In bacteria and eukaryotes, acetate can be used for acetyl-CoA production by the enzyme acetyl-CoA synthetase (ACS). Acetyl-CoA is the substrate for enzymatic as well as non-enzymatic acetylation of the amino group of lysine residues (König et al., 2014; Wagner and Payne, 2013). Lysine acetylation was even found to regulate the activity of ACS in *Salmonella enterica* (Starai et al., 2002). In addition, bacteria as well as green algae can produce acetyl-CoA from acetate by the two enzymes acetate kinase and phosphotransacetylase, which form a highly reactive acetyl-phosphate intermediate able to trigger lysine acetylation. In *E. coli*, the addition of acetate to the growth medium caused a strong increase in protein acetylation in the absence of the protein lysine deacetylase cobB, and was dependent on acetyl phosphate availability (Castano-Cerezo et al., 2014; Weinert et al., 2017). To reveal whether protein acetylation is affected by the carbon source availability in *Chlamydomonas*, we investigated the proteome and lysine acetylome dynamics of *Chlamydomonas* grown under phototrophic, mixotrophic, and heterotrophic growth conditions by using a stable isotope dimethyl-labeling technique followed by quantitative liquid chromatography mass spectrometry (LC-MS) analyses.

RESULTS

Lysine acetylation dynamics in *Chlamydomonas* is dependent on light and acetate

In order to analyze the impact of different growth conditions on the lysine acetylation status of *Chlamydomonas* proteins, a pre-culture of CC-3491 cells was grown under mixotrophic conditions with a medium light intensity (30 μmol $m^{-2}sec^{-1}$). The cells were then washed with acetate-free medium and used to inoculate the main cultures, which were grown under either heterotrophic, photoautotrophic, or mixotrophic conditions for 30 h (Figure 1a). The light intensity of the photoautotrophic and mixotrophic growth conditions was increased to 100 μmol m^{-2} sec^{-1} to support photosynthesis (Gorman and Levine, 1965; Harris, 1989). After 30 h of growth under the respective condition, the cells were harvested by centrifugation, shock-frozen in liquid nitrogen, and stored at −80°C until further analysis. We selected a 30-h cultivation time, since there was a visible difference in the acetylation status of a putative histone protein band (below 29 kDa) detectable on the Western blot between the light- and dark-grown cultures (Figure 1b). In addition, a prominent band between 45 and 66 kDa was visible, especially under heterotrophic conditions. This band most likely represents the large subunit (RbcL) of ribulose-1,5-bisphosphate carboxylase/oxygenase (RuBisCO), since it has previously been shown that RbcL is highly acetylated in Arabidopsis, especially during the night (Finkemeier et al., 2011; Gao et al., 2016).

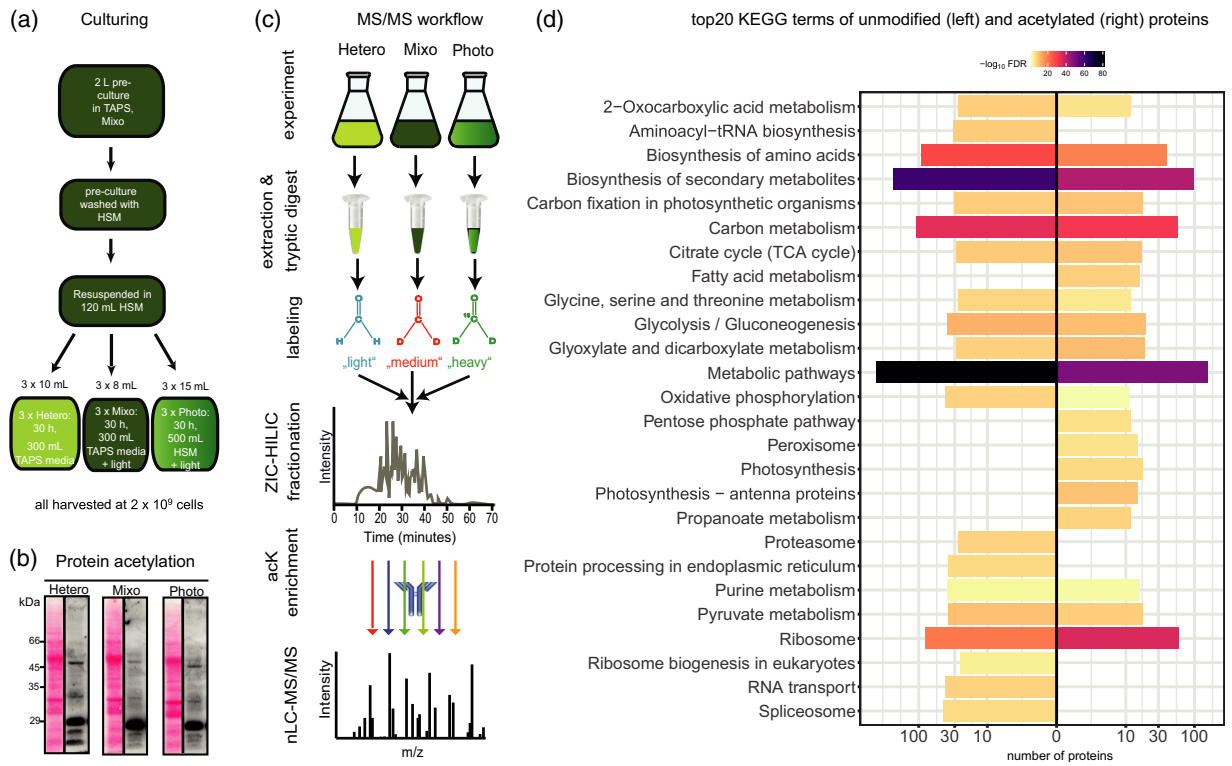

Figure 1. General overview of the experimental setup and proteomic analyses of *Chlamydomonas* cells from different growth conditions. (a) Culturing conditions. A common pre-culture was split into three specific growth conditions (hetero-, mixo-, and autotrophic, experiments performed in three biological replicates). Initial cell density was adjusted to compensate for different growth under the respective conditions and yield 2 × 10^9 cells at harvest. (b) Anti-acK Western blot of *Chlamydomonas* cell extracts (the Ponceau S stain is presented next to the blots as loading control). (c) LC-MS/MS workflow. After harvest, proteins were digested and isotopically labeled. Pooled peptide samples were pre-fractionated, enriched by immunoprecipitation of acK peptides, and analyzed by LC-MS/MS in addition to full proteome samples (in biological triplicates). (d) Overview of the top 20 KEGG pathways containing unmodified proteins identified in total extracts (bars to the left) and with an acK site (bars to the right). No bar is shown when the respective KEGG term was not among the top 20 terms ranked according to protein number per term and protein condition. $-\log_{10}$(FDR) from the functional enrichment analysis *via* StringDB are used as fill color.

Mass spectrometry-based profiling of the *Chlamydomonas* proteome and acetylome

The variety of lysine-acetylated proteins detected on the Western blot prompted us to quantify total proteome and acetylome changes under the different growth conditions in a large-scale MS-based shotgun proteomic approach combined with a stable isotope dimethyl-labeling strategy (Lassowskat et al., 2017). An overview of the MS-based workflow is shown in Figure 1(c). Samples from the three different growth conditions were analyzed in three biological replicates. Proteins from each replicate were extracted and digested with trypsin, and free amino groups of peptides were labeled with light, medium, and heavy stable isotope dimethyl forms, respectively. To prevent any labeling bias, a swap of the light, medium, and heavy dimethyl labels was performed on the third replicate. Equal amounts of the labeled peptides from the three growth conditions were combined and subjected to ZIC-HILIC fractionation to reduce the sample complexity (Giese et al., 2020). After fractionation, the samples were enriched for lysine-acetylated peptides by immunoaffinity purification. All fractions were analyzed on a Q-Exactive Plus (Thermo Fisher Scientific, Bremen, Germany) mass spectrometer and proteins and acetylation sites were identified and quantified using MaxQuant (Tyanova et al., 2016). In total, more than 5000 protein groups were identified with a protein false discovery rate (FDR) of <1%. The detected proteins have various functions in a broad variety of metabolic pathways according to the top 20 KEGG terms (Figure 1d, left). In addition, we identified almost 1400 lysine acetylation sites (acK sites) in total. Out of the top 20 KEGG terms, fatty acid and propanoate metabolism, the pentose phosphate pathway, peroxisomal microbodies, photosynthesis, and antenna proteins are exclusively enriched as functional terms within the acetylated proteins (Figure 1d, right).

Proteome changes depending on light and acetate

We first evaluated the protein abundance changes depending on the different growth conditions in a pairwise manner. For each condition, more than 4700 protein groups

were quantified in at least two replicates (Table S1). The different growth conditions affected the abundance of up to 30% of the protein groups in between treatments (regulated with a *p*-value of <0.05, Table 1, Figure 2a). The protein groups with an absolute value for the $\log_2$(fold change [FC]) of ≥1 and a corresponding *p*-value of <0.05, quantified in at least two replicates by their respective dimethyl ratios, were analyzed using StringDB for functional enrichment (Figure 2b,c).

In the comparison of heterotrophic to mixotrophic conditions (Figure 2b, left column), mainly proteins involved in photosynthesis are downregulated, while (motor) proteins associated with cell projection located in cilia and flagella are upregulated under heterotrophic conditions. A similar picture emerged when comparing the heterotrophic to photoautotrophic growth conditions (Figure 2b, middle column).

In the comparison of mixo- and phototrophic conditions (Figure 2b, right column), the StringDB analysis indicates that the photosynthetic machinery seems to vary to a lesser extent between those two states than in the comparisons of heterotrophic conditions to either one of them. It is mainly ribosomal proteins that are more strongly expressed under (purely) phototrophic conditions, whereas proteins associated with oxidative phosphorylation are upregulated under mixotrophic conditions accounting for the adaptations specific to these conditions (Figure 2b, right column).

Due to our experimental setup, we are not only able to make binary comparisons as just described, but also to evaluate protein changes that are specific to overlapping features, namely light and dark acclimation or CO_2 and acetate as carbon sources (Figure 2c). We first turned to proteins specific for the comparison of growth in the dark and the light by comparing the heterotrophically grown cells to those grown under the two other conditions. Acclimation to growth in the light (Figure 2c, top left) is accompanied by upregulation of proteins associated with photosynthesis, while in the dark, proteins associated with fatty acid degradation, peroxisomal microbodies, and the TCA cycle are higher in abundance. Pherophorins are upregulated (Figure 2c, bottom right), indicating a switch to sexual reproduction, which is typical for algae when grown under unfavorable conditions (Hallmann, 2011).

When comparing the phototrophic state to the two other growth conditions, one can gain insights into the proteome adjustments under fully autotrophic conditions compared to acclimation to an external carbon source. Acclimation to growth in the absence of an organic carbon source (Figure 2c, top right) is accompanied by upregulation of proteins associated with photosynthesis, including clusters that are associated with carbonic anhydrase, which is important to provide adequate CO_2 supply for photosynthesis (Tirumani et al., 2014; Ynalvez et al., 2008). In the presence of acetate as an external carbon source in the growth medium, proteins associated with the degradation of fatty acids and other organic compounds are significantly enriched (Figure 2c, bottom left).

We found 79 proteins to be significantly upregulated in both mixo- and heterotrophic conditions when compared to phototrophic conditions. These proteins are mainly related to acetate metabolism. An analysis of the best matching loci of *Arabidopsis thaliana* homologs via Stitch DB revealed that 18 of those are known to interact with acetate directly (Figure S1) (Szklarczyk et al., 2016).

There are 68 proteins downregulated under both conditions, whereof 14 are reported to be directly associated with CO_2 metabolism (Figure S2). In summary, under

Table 1 Summary of identified and quantified protein groups and lysine acetylation (acK) sites. For quantification of protein levels and acK sites, a ternary comparison between heterotrophic (Hetero), mixotrophic (Mixo), and photoautotrophic (Photo) growth conditions was made by pooling light, medium, and heavy dimethyl-labeled peptides from the respective growth condition in biological triplicates. Between biological replicates labels were swapped between conditions to prevent any labeling bias. Filters applied: 1% false discovery rate (FDR) at peptide-to-spectrum match (PSM), peptide, and protein levels. Filters applied for up- and downregulated features: values in minimum two out of the three biological replicates, LIMMA *p*-value <0.05

	Hetero/Mixo	Mixo/Photo	Hetero/Photo
Protein groups			
Quantified	5346	5340	5355
Up	1072	409	835
Down	552	705	670
5863 identified			
AcK sites			
Quantified	280	278	289
Up	32	40	55
Down	10	5	9
1376 identified			

Figure 2. Differential protein expression analysis of *Chlamydomonas* under different growth conditions. (a) Volcano plots correlating the $\log_2$(FC) values of protein groups and the respective $-\log_{10}$(*p*-values) from LIMMA statistical analyses. Only proteins quantified in at least two biological replicates are shown. The color gradient indicates the absolute value of the product of the $\log_2$(FC) and $-\log_{10}$(*p*-values). (b) Volcano plots for functional enrichment analysis performed with StringDB on either up- or downregulated proteins in the respective binary comparison using the website's 'Proteins with Values/Ranks - Functional Enrichment Analysis' function. Plots are shown correlating the number of proteins in specific functional terms enriched in either growth condition and the respective $-\log_{10}$(FDR) given by StringDB when testing for enrichment. (c) Scatter plot for functional enrichment for StringDB features that are shared or unique between different growth conditions: light (Mixo and Photo) versus dark (Hetero) (top left versus bottom right) and CO_2 (Photo) versus acetate (Hetero and Mixo) (top right versus bottom left). The respective number of proteins enriched in a term is shown on the *x*-axis and the $-\log_{10}$(FDR) resulting from the functional enrichment analysis by StringDB are given on the *y*-axis.

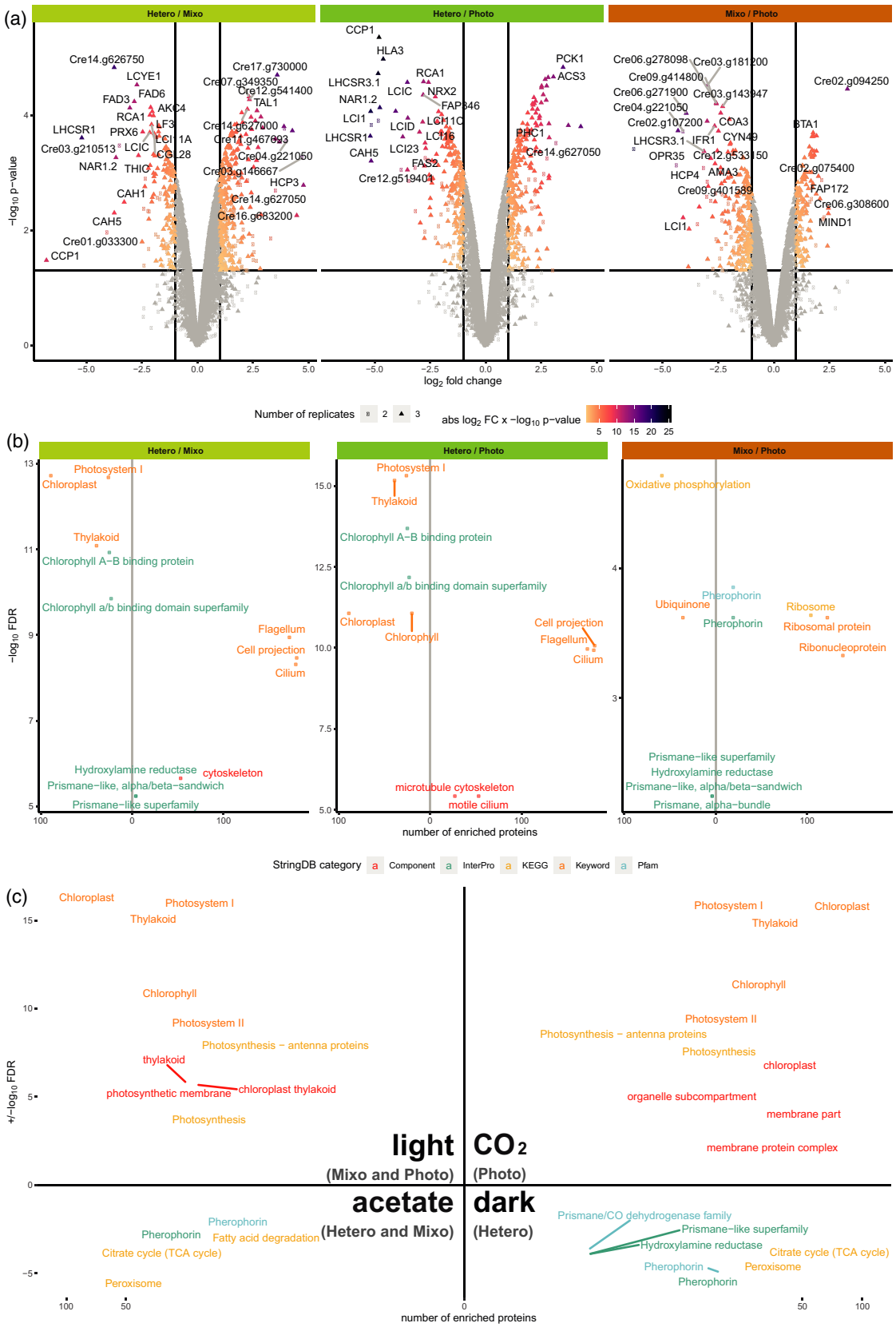

heterotrophic growth conditions, most photosynthesis- and chloroplast-related processes were downregulated. Upregulated proteins include those involved in fatty acid oxidation and the TCA cycle. By comparing the up- and downregulated proteins from the different growth conditions, novel protein regulations responding to either acetate and inorganic carbon or light and dark acclimation could be identified, such as the pherophorins.

Identification and functional annotation of lysine-acetylated proteins in *Chlamydomonas*

In total, 1376 acK sites were detected on 625 protein groups of *Chlamydomonas* (Table 1). For each of the binary comparisons between different growth conditions, more than 250 sites were quantified and more than half of those in at least two replicates (Table S2). We found about 15% of those sites to be significantly changed in their abundance. Under all three growth conditions, about 25% of the detected acK sites are found on proteins that were not detected and quantified as unmodified proteins under those conditions (Figure 3a,b). To investigate whether specific sequence motifs can be found surrounding the acK sites, the iceLogo tool was used to generate a sequence logo using the 15 amino acids on each site surrounding the acetylated lysine residue (Colaert et al., 2009). The sequence on top gives an overview of the sequence context for all detected acK sites. Amongst others, mainly glycine residues were generally overrepresented from −4 to +6 adjacent to the acetylated lysine residues (Figure 3c), as well as lysine at +4 and proline at −3 and +1. The sequence motifs surrounding the significantly differentially regulated acetylation sites also differ between the different growth conditions, probably indicating that different lysine deacetylases and acetyltransferases are active in *Chlamydomonas* depending on the available carbon sources (Figure 3c). Interestingly, the enrichment of glycine residues near the acetylation site disappears in the comparison of heterotrophic and mixotrophic growth conditions.

Lysine acetylation dynamics between heterotrophic, photoautotrophic, and mixotrophic growth conditions

To investigate the regulation of differential lysine acetylation between heterotrophic, photoautotrophic, and mixotrophic conditions a LIMMA statistical analysis was performed on the acetylated peptide ratios derived from the three biological replicates (Figure 4a, Table S2). The volcano plots in Figure 4(a) visualize changes in lysine acetylation between the different growth conditions. In addition, to distinguish the regulation at the level of the acetylated peptide from regulation of the total protein abundance, the protein ratios are plotted against the peptide ratios (Figure 4b). We focused our downstream analysis on the main metabolic pathways influenced by light and carbon source acclimations. Many proteins from central metabolic pathways were significantly changed in lysine acetylation levels as briefly outlined in the following (Figures 1e, 4c, and 5).

Heterotrophic versus mixotrophic growth conditions. In the comparison of heterotrophically and mixotrophically grown cells, light is the main difference between these two conditions, as both media contained acetate as carbon source. In total, 42 acK sites belonging to 31 unique protein groups were significantly differentially regulated in their abundance in heterotrophic compared to mixotrophic conditions (Figure 4a, left column). Under heterotrophic conditions several peroxisomal proteins such as enzymes of the glyoxylate cycle (malate synthase and citrate synthase), peroxin 11A, acetyl-CoA synthetase 3, and the multifunctional protein 2 involved in fatty acid beta-oxidation were increased in acetylation at several sites. In addition, acetylation of several chloroplastic proteins was affected. While proteins from the light reactions (AtpB and E, PsaB, PSAD, PSBO1, and LHCA1) showed a significant downregulation in their acetylation level under heterotrophic compared to mixotrophic conditions, enzymes of the Calvin-Benson cycle, such as glyceraldehyd-3-phosphate dehydrogenase, phosphoglycerate kinase, and RbcL (K175), showed a significant upregulation in their acetylation level. Among nuclear proteins, increased acetylation of a NuA4-domain acetyltransferase, a homeodomain-like/winged-helix DNA-binding family protein, the nuclear matrix protein THO1, and histone H2A was observed.

Heterotrophic versus photoautotrophic growth conditions. The comparison of heterotrophic versus photoautotrophic growth (Figure 4, middle column, Figure 5) showed the most distinct changes in lysine acetylation deriving from the diverging conditions with either an organic or inorganic carbon source. Photoautotrophically grown cells produce their energy by the fixation of inorganic CO_2 via the Calvin–Benson cycle. On this account, a total of 64 acK sites, belonging to 48 unique proteins, were significantly differentially regulated between heterotrophic and photoautotrophic conditions. The changes in lysine acetylation between heterotrophic and photoautotrophic conditions occurred on similar acK sites as the changes between heterotrophic and mixotrophic conditions, but were much more pronounced (up to 16-fold increase in lysine acetylation). The most affected pathways with several highly significantly differentially regulated acK sites are related to carbon metabolism, in particular those from fatty acid beta-oxidation and the glyoxylate cycle in peroxisomal microbodies, as well as from photosynthesis metabolism in chloroplasts. In Figure 5, an overview map of metabolism is presented depicting the relative changes in lysine acetylation normalized to protein abundance of the respective proteins. Although some of the peroxisomal enzymes were also strongly upregulated at the protein

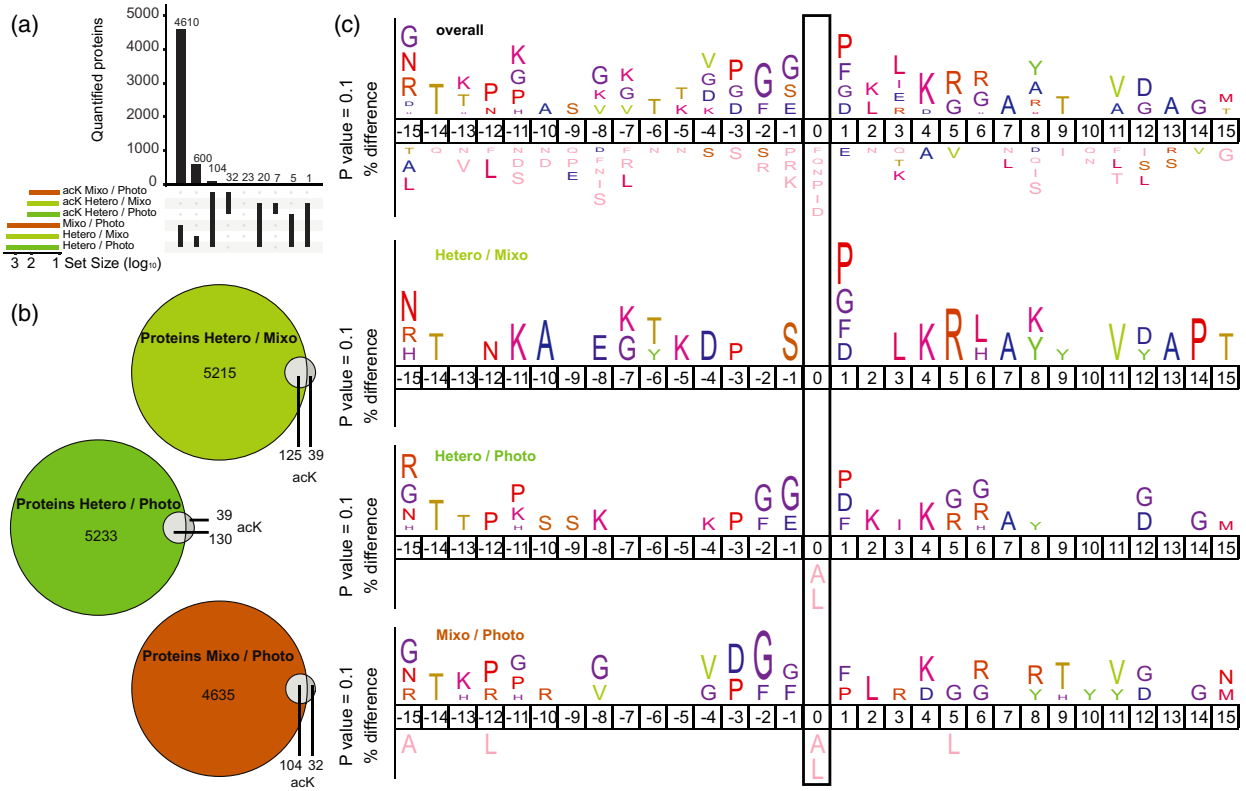

Figure 3. Comparison of the overlap of the unmodified, quantified proteins and proteins carrying a lysine acetylation site (a, b), and acetylation site motif analyses globally and per growth condition (c). (a) Upset plot for the overlap of unmodified, quantified proteins and proteins carrying an acK site under different growth conditions. Bars in the lower right panel indicate which binary comparisons overlap. (b) Venn diagrams presenting the overlap of unmodified proteins (colored) and proteins with acK sites (gray) per binary comparison between growth conditions. (c) Sequence context of all detected acK sites (top) and sequence windows found specifically differentially regulated in the respective binary comparison of growth conditions, comparing the frequency percentage of an amino acid at a certain location when acetylated. All motives are centered around the acK site, indicated by a box. The sequence logos were generated with the iceLogo tool (Colaert *et al.*, 2009).

level, the change in lysine acetylation levels for several of these proteins at multiple sites was considerably higher, indicating that a unique increase in lysine acetylation occurred for these proteins (Figure 4b, middle). For example, acetyl-CoA synthase 3 (ACS3) provides one of the entry points into the glyoxylate cycle pathway by producing acetyl-CoA from acetate in peroxisomal microbodies (Lauersen et al., 2016) (Figure 5). We identified two acK sites (K205 and K218) on ACS3, which were more than 16-fold increased under heterotrophic compared to photoautotrophic conditions. In the glyoxylate cycle, acetyl-CoA is then converted to citrate by the citrate synthase CIS2, which carried three strongly upregulated acK sites (K99, K340, and K446). While several acetylation sites were detected on the peroxisomal aconitase (ACH1) and isocitrate dehydrogenase (ICL1), none of them were quantifiable due to their low abundance (Table S1). A strong increase in lysine acetylation was observed under heterotrophic conditions on two out of 10 detected acK sites (K54 and K422) of malate synthase 1 (MAS1), which is the enzyme that converts succinate to malate in the glyoxylate cycle (Figures 4a,b and 5). Several additional peroxisomal and peroxisome-related proteins showed a strong increase in lysine acetylation, while the total protein level was only slightly increased. Interestingly, acetyl-CoA acyltransferase 1 (ATO1), which is related to beta-oxidation (Atteia et al., 2009; Goodenough et al., 2014), possesses three acetylation sites (K230, K274, and K232), which showed an up to 16-fold increase under heterotrophic conditions. In addition to proteins from the glyoxylate cycle, also other enzymes related to acetyl-CoA metabolism in different subcellular compartments showed an increase in acetylation under heterotrophic conditions. For example, dihydrolipoamide acetyltransferase 2 (DLA2) is a subunit of the plastidial pyruvate dehydrogenase complex and is involved in the conversion of pyruvate to acetyl-CoA as well as in the translation of *psbA* mRNA, which encodes a reaction center protein of photosystem II (PSII) (Bohne et al., 2013). DLA2 carries in total eight acK sites, including one (K197) that is significantly upregulated under heterotrophic and mixotrophic compared to photoautotrophic conditions, while the DLA2 protein level is unaltered under

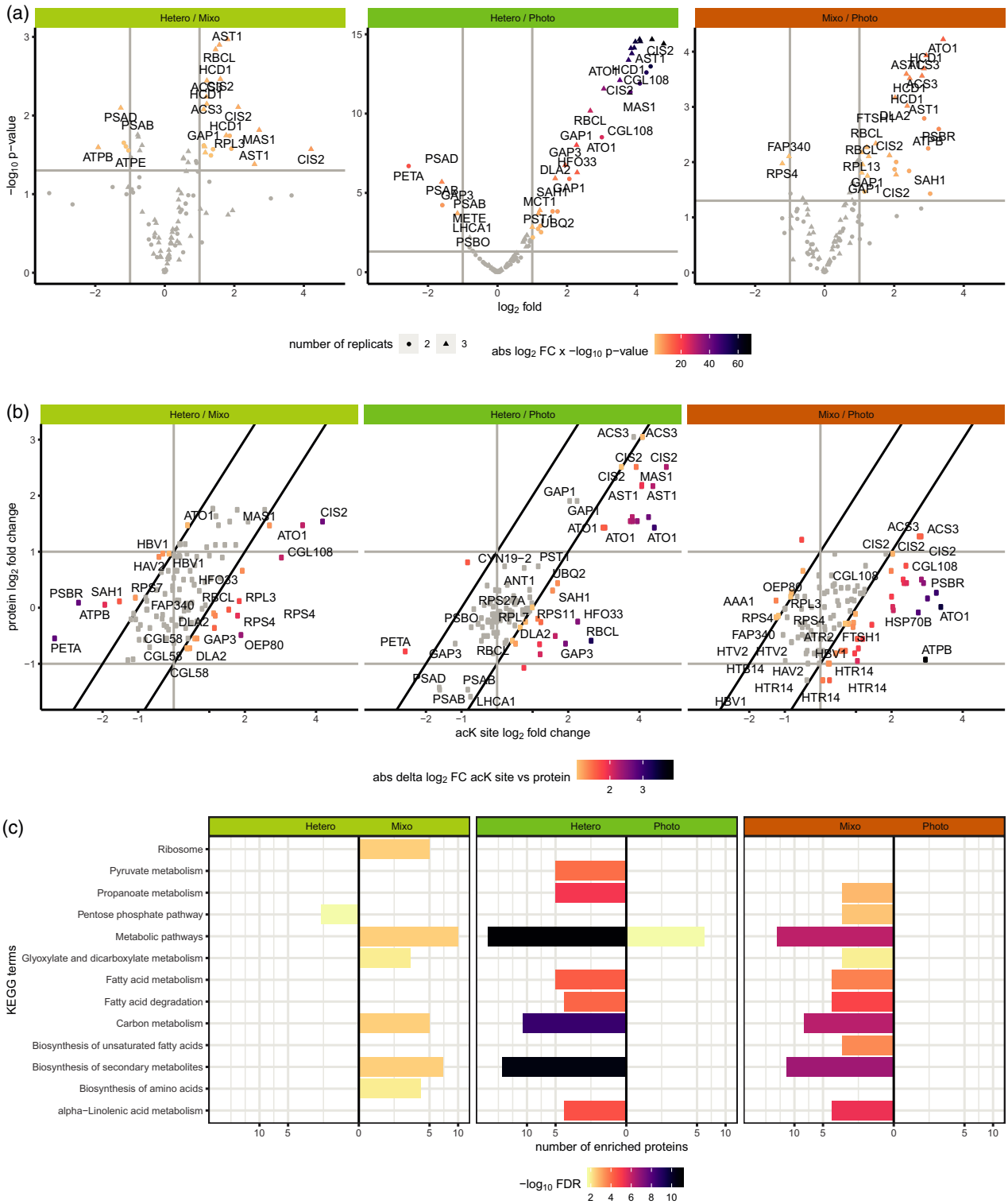

Figure 4. Quantitative profiling of regulated acetylation sites depending on growth conditions in *Chlamydomonas*. (a) Volcano plots correlating the $\log_2$(FC) values of acK sites and the respective $-\log_{10}$(p-values) from LIMMA statistical analyses for the comparison of different growth conditions. Only sites quantified in at least two replicates are shown. A color gradient indicates the absolute value of the product of the $\log_2$(FC) and $-\log_{10}$(p-values). (b) Scatter plots correlating the acK and protein FC values for different growth conditions. The color gradient indicates the difference in $\log_2$(FC) values for proteins and acK sites. The vertical reference line indicates log(FC) = 0 for acK site changes, the horizontal reference lines indicate $\log_2$(FC) = ±1 for proteins, and diagonal reference lines with slope = 1 and intercept = ±1 represent the difference between acK and protein FC values. (c) Functional enrichment analysis performed with StringDB on differentially acetylated proteins. Box plots correlate the number of acetylated proteins per KEGG term enriched in either growth condition. The number of proteins per term is depicted on the *x*-axis and the respective $-\log_{10}$(FDR) are shown as fill color of the respective bar.

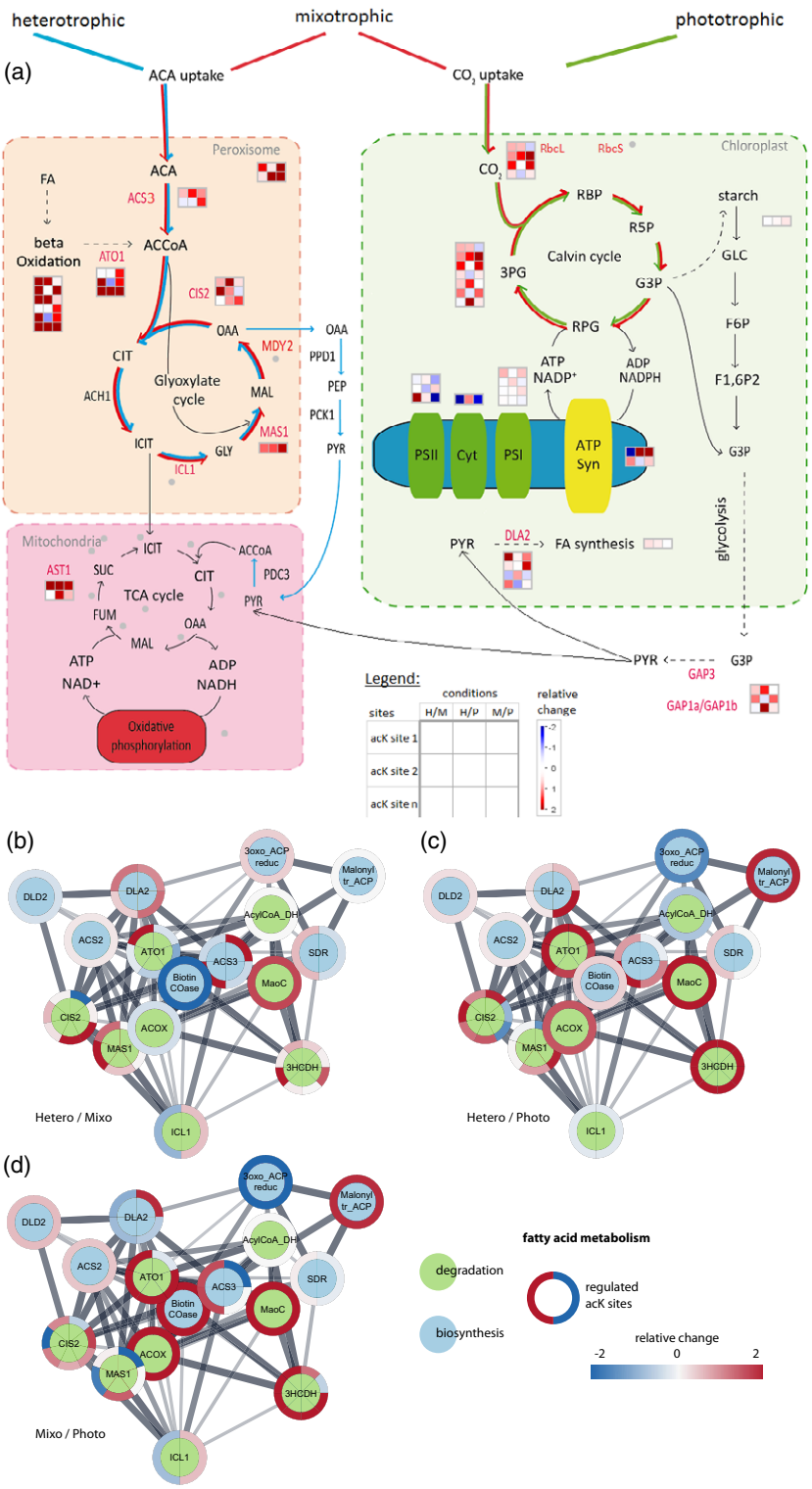

Figure 5. Effect of lysine acetylation on *Chlamydomonas* metabolism. (a) Metabolic map of carbon metabolism showing enzymes, protein complexes, and pathways in different compartments. (b–d) Protein–protein interaction (PPI) networks of proteins associated with fatty acid metabolism. (a–d) Log_2(FC) values of acK sites normalized to protein levels between different growth conditions. Downregulated sites are shown in blue and upregulated sites in red. Each box in (a) represents a protein, protein complex, or pathway as indicated. Each row of three squares represents one acK site. The three columns represent the log_2(FC) values of an acK site in the binary comparison of the growth conditions: heterotrophic and mixotrophic (H/M), heterotrophic and photoautotrophic (H/P), and mixotrophic and phototrophic (M/P). In the PPI networks in (b–d), the changes in normalized acK status are given as rings surrounding the proteins. Rings are split if more than one acK site was detected for a protein. The inner circle is colored depending on whether a protein is involved in fatty acid degradation (green) or biosynthesis (blue). Visualization for (a) was performed with MapMan (Thimm *et al.*, 2004) while (b–d) were created using Cytoscape (Shannon *et al.*, 2003).

these conditions (Figure 4b) (Bohne et al., 2013). Fifteen acK sites were identified on the large subunit of RuBisCO (RbcL), of which six could be quantified. Again, K175 of RbcL showed a strong and significant upregulation in acetylation under heterotrophic conditions.

Mixotrophic versus photoautotrophic growth conditions. When comparing mixotrophic and photoautotrophic growth conditions, acetate is the main factor which influences lysine acetylation. In total, 45 acK sites from 32 unique proteins were significantly differentially

regulated in the comparison of the two conditions. Again, eight of these 32 proteins, which showed a strong increase in acetylation, were peroxisomal proteins involved in lipid breakdown. Remarkably, the lysine-acetylated proteins showed only minor changes in their total protein abundance (Figure 4b, right, $|\log_2(FC)| \leq 1$, Figure 5), indicating that the protein expression of the enzymes from the glyoxylate cycle is mainly controlled by light/dark acclimation, but not by acetate. Increased acetylation under mixotrophic growth conditions was identified on ADH1, which is a key enzyme in fermentative metabolism (Magneschi et al., 2012). Under these conditions also Calvin–Benson cycle enzymes and proteins involved in the light reaction showed an increase in acetylation in the presence of acetate in the light. Among the photosynthetic proteins, the PSBR protein from PSII showed a more than eightfold and significant upregulation in lysine acetylation on K38 in the presence of acetate and light (Figure 4a,b, right column). PSBR is required for efficient binding of the light-harvesting complex (LHC) protein LHCS3 to PSII in *Chlamydomonas*, and hence PSBR acetylation could be important for PSII–LHCII_LHC3 supercomplex formation and thermal dissipation in the light (Xue et al., 2015).

Lysine acetylation on enzymes involved in carbon and fatty acid metabolism

We performed a functional enrichment analysis with StringDB to evaluate to which pathways the proteins belong for which the acK status was altered (Figure 4c). When comparing the proteins with altered acetylation levels between algae grown under phototrophic conditions and those grown in the presence of acetate in the medium, it becomes clear that proteins responsible for carbon and fatty acid metabolism were affected (Figure 4c, middle and right panels). When directly comparing proteins with altered acK status between the mixo- and heterotrophic states, proteins connected to the ribosome and amino acid biosynthesis show increased acetylation when light was available (Figure 4c, left).

We went on to evaluate the effect of lysine acetylation on fatty acid metabolism in more detail (Table S4). We found 16 proteins with differentially acetylated lysines under the different growth conditions that also form a highly connected interaction network (Figure 5b–d). Six of those proteins play a role in fatty acid biosynthesis (blue circles), while the other 10 are associated with fatty acid degradation (green). Both catabolic and anabolic enzymes show a high degree of acetylation. Especially 3-hydroxyacyl-CoA dehydrogenase (3HCDH), involved in fatty acid degradation, carries eight acK sites, which show stronger acetylation in the presence of acetate and with no light available (Figure 5c,d). The biotin carboxylase subunit (biotin COase) of the polymeric acetyl-CoA carboxylase complex is acetylated to a higher extent when comparing photo- to mixotrophic or to heterotrophic growth. Ketoacyl-ACP reductase shows a strong decrease in acetylation when comparing phototrophic growth to the other two conditions.

The large subunit of RuBisCO and citrate synthase show a strong increase in lysine acetylation occupancies under heterotrophic conditions

To get an impression of lysine acetylation occupancies on *Chlamydomonas* proteins, we selected the highly regulated acK site K175 of RbcL, since increased lysine acetylation was reported previously for RuBisCO during the night in Arabidopsis, which resulted in a significant downregulation in RuBisCO activity (Finkemeier et al., 2011; Gao et al., 2016). The concept of site occupancy calculation for PTMs was initially presented by Olsen and co-workers for phosphorylated peptides (Olsen et al., 2010). It assumes that in different conditions modified peptides should have their abundance changed inversely proportional to their non-modified counterpart. In the case of acK sites this is not easily possible, since the acetylation is masking the positive charge of the side chain, which would lead to a tryptic cleavage. Hence, the modified and unmodified peptides are of very different lengths and the unmodified peptides might contain too few amino acids for an unambiguous identification. However, in case both peptides can be detected, the increase in abundance of the acetylated peptides between two conditions can be calculated relative to the decrease in their non-modified counterparts carrying a missed cleavage at the site of interest (Nakayasu et al., 2014). We made use of this fact in our calculations. Figure 6(a) shows that the peptide GLLGCTIKPK was detected in its acetylated form on position K8 in all three dimethyl labeling states. The peptide was also detected with one missed cleavage in its unmodified form, probably due to the presence of proline. Hence, we were able to calculate the occupancy for this particular site of K175 of RbcL using the ratios for the acetylated and the corresponding unmodified peptide that has not been cleaved at K175. The occupancy was the highest (35%) in the algae grown heterotrophically without light. This site shows the lowest occupancy (only 6%) in the phototrophically grown *Chlamydomonas* cultures, indicating active deacetylation (Figure 6a). In addition to RbcL, we also evaluated the occupancy of two acK sites (K99 and K340) on the peroxisomal citrate synthase CIS2, where corresponding unmodified peptides were detected. In the case of CIS2 we calculated the occupancies based on dimethyl ratios for acetylated and unmodified peptides not cleaved at the respective positions as outline before. For another strongly acetylated site (K446) on CIS2 no unmodified counterpart was detected, and hence no occupancy could be calculated. CIS2 is a key enzyme of the glyoxylate cycle and catalyzes the conversion of acetyl-CoA to citrate. The enzyme

showed a strong increase in acetylation that was dependent on acetate in the growth medium (Figures 4 and 5). The occupancy calculation revealed that K99 is acetylated to about 50% under heterotrophic conditions. A lower occupancy was observed under mixo- (33%) and phototrophic (21%) growth conditions (Figure 6b). In a sequence alignment, this amino acid position turns out to be conserved in algae; however, in land plants such as *A. thaliana*, this position is exchanged to a negatively charged glutamic acid (Figure S3a). The acK site K340 of CIS2 was almost fully acetylated when the algae were grown without any light (heterotrophically). The occupancy level was reduced to 41% under mixo- and to 9% under phototrophic conditions, again indicating active deacetylation. The lysine residue K340 is highly conserved amongst plants in general. To investigate whether the acetylation occupancy correlated with the activity of citrate synthase, we determined the total citrate synthase activity in protein extracts from all three growth conditions (Figure 6c). It must be noted that next to the peroxisomal CIS2, a mitochondrial CS isoenzyme (CIS1) exists in *Chlamydomonas*, which however showed no significant change in protein abundance under the investigated conditions (Table S1). The total citrate synthase activity was increased more than 2.2-fold under heterotrophic compared to photoautotrophic growth conditions, which corresponds with the strong increase in protein abundance (5.6-fold) as well as an even stronger increase in lysine acetylation (11- to 25-fold) of CIS2 (Figure 4b, Table S1).

DISCUSSION

In recent years, several global acetylome characterizations have been reported both in prokaryotes and eukaryotes (Choudhary et al., 2014). The present study presents the *Chlamydomonas* acetylome in combination with a stable dimethyl-labeling technique to compare heterotrophic, photoautotrophic, and mixotrophic growth conditions. Mixotrophic growth conditions promote optimal lipid formation, which is important for large-scale generation of algal-based biofuels (Sager and Granick, 1953; Work et al., 2010). It is known that the addition of acetate to the growth medium boosts metabolism and leads to a higher growth rate in several green algae (Lauersen et al., 2016; Rai et al., 2013; Smith et al., 2015). In *Euglena gracilis* the number of microbodies increased in the presence of acetate (Graves et al., 1971). This is in accordance with the finding that the total volume of peroxisomal microbodies and the transcript levels of enzymes involved in the glyoxylate cycle increased when *Chlamydomonas* cells were grown on acetate-containing medium (Hayashi et al., 2015). Strikingly, genes belonging to the GPR1/FUN34/YaaH (GFY) superfamily also showed increased expression upon

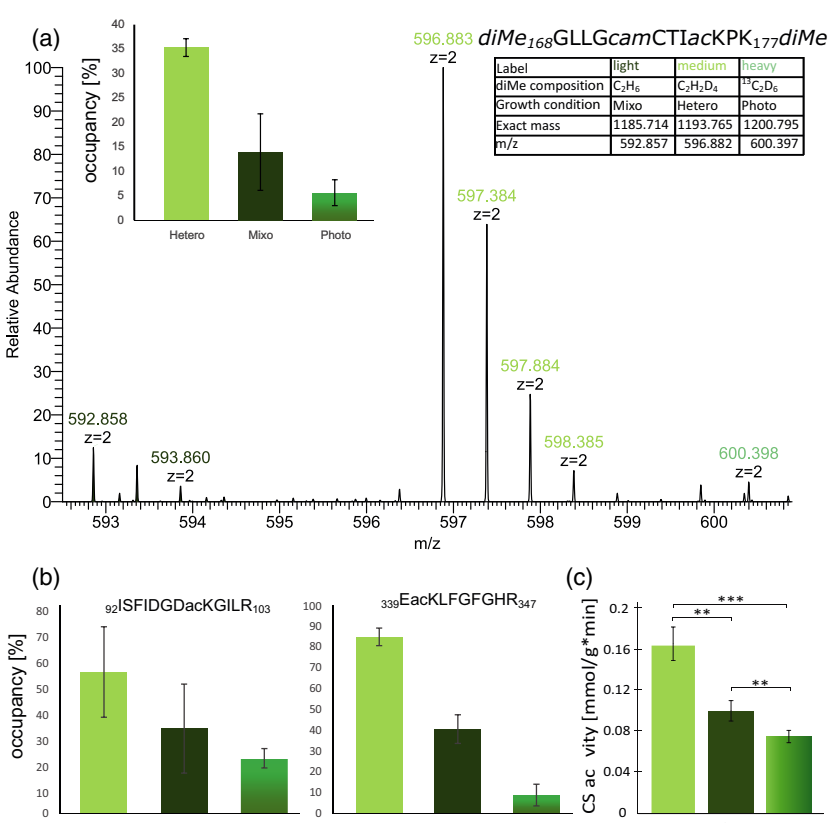

Figure 6. AcK site occupancies and enzyme activity. (a) AcK site occupancy of K175 of RbcL (detected in a peptide spanning G168–K177 of RbcL). The table indicates mass details and the labeling scheme of the detected dimethyl-labeled acK peptide of RbcL, as shown in the zoomed in panel of the labeled triplet in the MS^1 spectrum. The bar graph shows average site occupancies ± standard deviation (SD) (n = 3). (b) Bar graph of acK site (K99 left [I92–R103], K340 right [E339–R347]) occupancies for the peroxisomal citrate synthase CIS2. The respective numbers of the first and last amino acids are also given in the figure. Replicate values are shown in Table EV3. (c) Total enzymatic activity of citrate synthase (CS) in *Chlamydomonas* protein extracts from different growth conditions ± SD (n = 3). Significant differences are indicated with asterisks (Student's t-test, p-value < 0.05).

acetate addition. CrGFY1–5 show structural similarity to bacterial succinate-acetate channels and specifically localize to microbodies. GFY3–5 expression was strongly upregulated in the presence of acetate, and they were found to be co-expressed with genes participating in acetate metabolism especially with those involved in the glyoxylate cycle (Durante et al., 2019). Also in this study, we observed a strong increase in abundances of proteins involved in the glyoxylate cycle, as well as of the GFY3–5 proteins, particularly under heterotrophic conditions. Thus, these results provide further confirmation that peroxisomal microbodies play a key role in acetate assimilation (Lauersen et al., 2016). A recent metabolomic and proteomic study in *Isochrysis galbana* showed that fatty acids accumulated when the algae were fed with acetate. The enzymes acting in the glyoxylate cycle accumulated when the medium was supplemented with acetate and nitrogen but not under nitrogen starvation conditions. Hence, the acetate-dependent regulation relies on nitrogen availability (Kaur et al., 2021). To further improve biofuel production, it is of great interest to understand the underlying principles of metabolic pathway regulation in *Chlamydomonas*. The acetylome data which we present here provide new possible regulatory mechanisms based on this PTM. However, it is important to note that a change in acetylation status does not necessarily mean that the activity or function of this protein is also regulated by this modification. This depends on whether the site of modification is essential for protein function, which needs to be confirmed in a case-by-case manner for every protein and modification site (Hosp et al., 2017). By using an MS-based approach, we identified an overall number of 5863 protein groups with 1376 acK sites (Table 1). Our data indicate that lysine acetylation occurs on proteins involved in diverse metabolic pathways in *Chlamydomonas*, which is in accordance with observations from several other organisms (Cobbold et al., 2016; Fang et al., 2015; Finkemeier et al., 2011; Hartl et al., 2017; Henriksen et al., 2012; Liu et al., 2014; Uhrig et al., 2019; Wu et al., 2011; Zhou et al., 2018). The widespread distribution recapitulates the vital biological function of this PTM, and includes metabolic enzymes involved in protein biosynthesis and photosynthesis, as well as several important carbon utilization pathways, such as glycolysis, the TCA cycle, and the glyoxylate cycle. Here we investigated the influence of acetate and inorganic carbon, as well as light availability on lysine acetylation of proteins in *Chlamydomonas*, thereby allowing to uncover the possible regulatory function of this modification. Our data show that acetate as carbon source has a major influence on lysine acetylation of selected nuclear, peroxisomal, and plastid proteins, as indicated by the large changes in lysine acetylation, when comparing either heterotrophic or mixotrophic with photoautotrophic conditions (Figure 4). Since acetate can be converted to acetyl-CoA via ACS and ACK in *Chlamydomonas*, it can be speculated that lysine acetylation plays a major role in causing changes in the activity of metabolic enzymes, which direct the metabolic flux to produce energy from acetate (Yang et al., 2014). Especially the enzymes of the glyoxylate cycle showed a strong increase in the total proteome and an even stronger increase in their acetylation levels. This supports previous findings that acetate enters the glyoxylate cycle pathway in peroxisomal microbodies of *Chlamydomonas*, which is the preferred carbon utilization pathway especially for heterotrophically grown cells (Plancke et al., 2014, Lauersen et al., 2016). In addition, the strong upregulation of enzymes involved in the glyoxylate cycle under heterotrophic conditions could be necessary because during longer periods of darkness plants start degrading their endomembrane system and depend on fatty acid beta-oxidation (Kunze et al., 2006). Additionally, the number of peroxisomal microbodies increases with acetate in the media (Hayashi et al., 2015). In Arabidopsis peroxisomal proliferation is regulated by an increased abundance of PEX11 proteins (Lingard and Trelease, 2006). Here we observed an increase in acetylation of PEX11a under heterotrophic conditions (Table S2), which could be important for regulation of PEX11 function. The link between acetate metabolism and lysine acetylation is well studied and is mainly established because of the known activity regulation of ACS by lysine acetylation in several organisms (Crosby et al., 2010; Gardner et al., 2006; Starai et al., 2002). While in *Salmonella enterica* Lys609 is actively acetylated by the acetyltransferase Pat and thereby inactivated (Starai and Escalante-Semerena, 2004), this lysine site, although it is conserved in *Chlamydomonas*, was not affected in our study (Figure S3b). Thus, it remains to be discovered whether the highly increased acetylation on ACS3, as well as on many other enzymes of the glyoxylate cycle, which we observed when acetate is present resulted from active acetylation via an acetyltransferase or from chemical acetylation as a by-product from acetyl-P production via ACK as in *E. coli* (Castano-Cerezo et al., 2014). While acetylation of metabolic enzymes is more often reported in the context of inhibition of enzyme activity, activation of an enzyme by this PTM was reported for the glycolytic activity of the *E. coli* glyceraldehyd-3-phosphate dehydrogenase, enoyl–coenzyme A hydratase/3-hydroxyacyl–coenzyme A dehydrogenase in fatty acid beta-oxidation, the TCA cycle enzymes aconitase and malate dehydrogenase in human liver and heart tissue, respectively, and malate dehydrogenase from Arabidopsis and *Physcomitrella* (Balparda et al., 2021; Fernandes et al., 2015; Finkemeier et al., 2011; Wang et al., 2010; Zhao et al., 2010). Hence, it cannot be easily predicted whether acetylation has a positive or negative effect on enzyme function, because the effect on activity or function is highly dependent on the position of the acetylation site within the protein structure (Hartl et al., 2017; Hosp et al., 2017; Schmidt

et al., 2017). In addition, the site stoichiometry of acetylation on a given enzyme within a cellular context can be important, and generally lysine acetylation was reported to occur only at sub-stoichiometric levels on most sites under the analyzed conditions (Hansen et al., 2019; Weinert et al., 2017). However, site stoichiometry analyses in an *E. coli* deacetylase mutant revealed that metabolic enzymes which either utilize or generate acetyl-CoA show occupancy rates of up to 98% on selected enzymes (Baeza et al., 2014), and acetyl-phosphate-dependent acetylations were responsive to changes in carbon flux (Schilling et al., 2015). Here we identified particularly high acetylation site occupancies for RuBisCO and peroxisomal citrate synthase under heterotrophic conditions (Figure 6). A strong negative impact of lysine acetylation on RuBisCO initial activities has previously been observed in *A. thaliana* (Finkemeier et al., 2011), and since K175 is a catalytically active site and responsible for protonation of the acid carboxylate, acetylation of K175 would inactivate RuBisCO activity (Knight et al., 1990). It will be interesting to investigate whether K175 acetylation is an evolutionarily conserved mechanism that inhibits RuBisCO in cells grown under heterotrophic growth conditions and whether this modification also prevents the degradation of the enzyme under these conditions. Especially for site stoichiometry analyses, single-cell algae will be particularly useful since they can be grown in a highly synchronized manner under standardized growth conditions. In addition to RuBisCO, the peroxisomal citrate synthase CIS2 showed occupancy levels of up to 85%, which correlated with high activities of total cellular citrate synthase (Figure 6). In future studies, it would be interesting to perform site-directed mutagenesis on the different acK sites of CIS2 and to identify the putative acetyltransferases and deacetylases in peroxisomal microbodies and chloroplasts of *Chlamydomonas*.

In conclusion, *Chlamydomonas* proved to be an excellent organism to study PTM-mediated regulation of proteins, which might be important for engineering algal and plant metabolism via genetic manipulations of their acK sites.

EXPERIMENTAL PROCEDURES

Algal strain and culture conditions

For *Chlamydomonas*, we used the cell wall-deficient strain CC-3491 cw15 *mt-* (Chlamydomonas Resource Center), which showed a reduced abundance of acetylated tubulin due to a high proportion of non-flagellated cells. The strain was maintained on 0.8% agar-solidified Tris/acetate/phosphate (TAP) medium (Harris, 1989) at 25°C under constant light (30 μmol m^{-2} sec^{-1}). Liquid cultures were incubated under agitation at 25°C. For analysis, a pre-culture was grown in 2 L of TAP medium containing 1% sorbitol (TAPS) to a density of approximately 5×10^6 cells/ml. Cells were harvested by centrifugation (5 min, room temperature, 1000 ***g***), washed once with 200 ml high-salt minimal medium (HSM), and resuspended in 120 ml HSM (approximately 8×10^7 cells ml^{-1}) (Sager and Granick, 1953). Considering different doubling times of *Chlamydomonas* cells under the selected growth conditions we used adjusted cell numbers for inoculation to reach a final cell number of approximately 2×10^9 cells after 30 h of growth per replicate. The suspension was used to inoculate the following cultures. For heterotrophic growth, 3×10 ml resuspended culture was used to inoculate 3×300 ml TAPS; for mixotrophic growth, 3×8 ml was used to inoculate 3×300 ml TAPS; and for growth under photoautotrophic conditions, 3×15 ml was used to inoculate 3×500 ml HSM to compensate for different growth rates under the applied conditions and to reach approximately the same final cell densities after 30 h. For mixotrophic and photoautotrophic growth, cells were then incubated in the light (100 μmol m^{-2} sec^{-1}), and cells were kept in complete darkness for heterotrophic growth. Cells were harvested by centrifugation, immediately frozen in liquid nitrogen, and stored at −80°C until further use.

Immunoenrichment and Western blot analysis

Cells were harvested by centrifugation and lysed by resuspending them in 2 ml basic extraction buffer (BEB) containing 50 mM Tris pH 7.5, 150 mM NaCl, 10% (v/v) glycerol, 2 mM EDTA, 0.5% (w/v) Triton X-100, and 5 mM dithiothreitol and protease inhibitor cocktail (cOmplete Tablets, Roche, Mannheim, Germany) by continuous pipetting. Additionally, to avoid deacetylation of proteins, 3 μM apicidin and 1 mM nicotinamide were added to the extraction buffer. For immunoenrichment of lysine-acetylated proteins, 200 μg protein extract was incubated with 20 μl anti-acetyl lysine antibody immobilized on agarose beads (ImmuneChem Pharmaceuticals, Burnaby, BC, Canada) for 3 h at 4°C. Immunoprecipitates were washed three times with extraction buffer and eluted by boiling in gel loading buffer for 5 min. For Western blot analysis, proteins were separated by SDS-PAGE, transferred to a nitrocellulose membrane, and probed using an acetyl lysine antibody in a 1:1000 (v/v) dilution (ImmuneChem Pharmaceuticals, Burnaby, BC, Canada). Horseradish peroxidase-conjugated secondary antibody (Bio-Rad, Feldkirchen, Germany) was used in a 1:10 000 dilution.

Protein extraction and peptide preparation

Protein pellets from *Chlamydomonas* were extracted in 10 ml heated SDT lysis buffer containing 4% (w/v) SDS, 100 mM Tris/HCl pH 7.6, and 10 mM DTT for 10 min at 95°C with occasional mixing followed by 15 min of sonication. Protein extracts were cleared by centrifugation and the protein amount was determined using the 660 nm Pierce protein assay with compatibility reagent (Pierce, Rockford, IL, USA) as previously described (Hartl et al., 2015).

To remove excess SDS and to prepare samples for tryptic digestion, the FASP method with Amicon Ultra-15 centrifugal filter units (Millipore, Darmstadt, Germany) was used (Wisniewski et al., 2009). Briefly, 10 mg of the protein extract was diluted with 8 M urea in 100 mM Tris/HCl pH 8 until an SDS concentration of <0.5% was reached. After SDS removal, the extract was alkylated using 50 mM iodoacetamide for 30 min in the dark, excess reagent was washed through a filter, and the buffer was replaced with 50 mM NH_4HCO_3. The reduced and alkylated proteins were digested using MS-grade trypsin (T6567, Sigma-Aldrich, Darmstadt, Germany) in an enzyme-to-protein ratio of 1:100. Eluted peptides were quantified at 280 nm. Digested peptides were dimethyl-labeled on C_{18} Sep-Pak plus short columns (Waters, Eschborn, Germany) as previously described (Lassowskat et al., 2017). Equal amounts of light, medium, and heavy dimethyl-labeled peptides were pooled for each replicate and the solvent was evaporated in a vacuum centrifuge. The dried peptides were dissolved in 1 ml TBS buffer (50 mM Tris-HCl, 150 mM NaCl, pH 7.6) and pH was checked and adjusted if required. Peptides (15 μg) were stored for whole proteome analysis. About 10 mg of the pooled labeled peptides were

resuspended in 2 ml 95% solvent A (95% acetonitrile, 5 mM ammonium acetate) and 5% buffer B (5 mM ammonium acetate) and fractionated with a flow rate of 500 $\mu l\ min^{-1}$ on a Sequant ZIC-HILIC column (3.5 μm, Merck, Darmstadt, Germany) using a segmented linear gradient of 0–60% solvent B (5 mM ammonium acetate). The fractions were combined to seven final fractions and dried in a vacuum centrifuge. Peptides were resuspended in IP buffer (50 mM Tris/HCl pH 7.6, 150 mM NaCl) and the concentration was determined on a spectrophotometer at 280 nm. Lysine-acetylated peptide enrichment was performed as previously described with 1 mg peptide per fraction (Lassowskat et al., 2017). After enrichment, the eluted peptides were desalted using C_{18} Stagetips and dried in a vacuum centrifuge.

Mass spectrometry

Dried peptides were redissolved in 2% acetonitrile (ACN), 0.1% trifluoroacetic acid for analysis. Total proteome samples were adjusted to a final concentration of 0.2 $\mu g\ \mu l^{-1}$. Samples were analyzed using an EASY-nLC 1000 (Thermo Fisher Scientific) coupled to a Q Exactive Plus mass spectrometer (Thermo Fisher). Peptides were separated on 16-cm frit-less silica emitters (New Objective, Littleton, MA, USA, 0.75 μm inner diameter), packed in-house with reversed-phase ReproSil-Pur C_{18} AQ 3 μm resin (Dr. Maisch, Ammerbuch, Germany). Peptides (5 μl) were loaded on the column and eluted for 120 min using a segmented linear gradient of 0–5% solvent B (solvent A 5% ACN, 0.5% formic acid [FA]; solvent B 100% ACN, 0.5% FA) at a flow rate of 250 $nl\ min^{-1}$. Mass spectra were acquired in data-dependent acquisition mode with a top 15 method. MS spectra were acquired in the Orbitrap analyzer with a mass range of 300–1750 m/z at a resolution of 70 000 full width at half maximum (FWHM) and a target value of 3×10^6 ions. Precursors were selected with an isolation window of 1.3 m/z. HCD fragmentation was performed at a normalized collision energy of 25. MS/MS spectra were acquired with a target value of 10^5 ions and an intensity threshold of 7.3×10^5 (acetylated peptides) or 1.1×10^5 (total proteome samples) at a resolution of 17 500 FWHM and a fixed first mass of $m/z = 100$. Peptides with a charge of +1, a charge of > +6, or an unassigned charge state were excluded from fragmentation for MS^2. Dynamic exclusion for 30 sec prevented repeated selection of precursors.

MS/MS data analysis

Raw data were processed using MaxQuant software (version 1.6.14.0, http://www.maxquant.org/) (Cox and Mann, 2008) with standard settings and the match-between run and re-quantification option enabled (Cox et al., 2014). The MS ratio count was set to a minimum of two and only unmodified peptides were used for protein quantification. MS/MS spectra were searched by the Andromeda search engine (integrated in MaxQuant) against the Phytozome 13 database for genomically encoded proteins (Creinhardtii_281_v5.6) supplemented with organelle-specific FASTA files for mitochondrial and plastidial sequences obtained from the NCBI GenBank (Goodstein et al., 2012; Merchant et al., 2007). Sequences of 248 common contaminant proteins and decoy sequences were automatically added during the search. Data of the total proteome and acetyl lysine-enriched samples were separated into two parameter groups to permit combined analysis. Dimethylation of peptide N-termini and lysine residues were set as light (H_4C_2), medium (D_4C_2), and heavy ($-H_2 + D_6{}^{13}C_2$) labels. Trypsin specificity was required and a maximum of two or four missed cleavages was allowed for total proteome and acetyl lysine-enriched samples, respectively. Minimal peptide length was set to seven amino acids. Carbamidomethylation of cysteine residues was set as fixed, with oxidation of methionine and protein N-terminal acetylation as variable modifications. Acetylation of lysine was added as a variable modification for the antibody-enriched samples. Allowed mass deviation was 4.5 ppm for peptides and 20 ppm for fragments. The minimum score and delta score for modified peptides were filtered for a minimum Andromeda score of 35 and 6, respectively. Peptide–spectrum matches and corresponding proteins were retained if they were below a false discovery rate of 1% as estimated using a target-decoy approach from a reversed sequence database. Localization probabilities of acetylated peptides are given in Table S2. Subsequent data analyses were performed in R. The LIMMA 3.42.2 package was used to determine differentially regulated proteins and acetylation sites (Ritchie et al., 2015) in R 3.6.2 (R Core Team, 2016). Volcano plots were generated with ggplot2 3.3.0, plotting the ($-\log_{10}$-transformed) non-adjusted p-values versus the $\log_2$(FC) values. The iceLogo web server was used for sequence logo creation (Colaert et al., 2009). A local blast was used in order to map the protein entries from Phytozome and the NCBI GenBank to String identifiers. String's 'Proteins with Values/Ranks - Functional Enrichment Analysis' was used to analyze the log(FC) values from full proteome experiments, while pre-filtered lists were used for functional enrichment and protein–protein interaction network analysis for acetylation sites. Mercator4 was used for functional annotation and classification of the significantly differentially regulated acK sites (Schwacke et al., 2019). The protein sequence information used for identification was uploaded to the website for annotation and the resulting mapping was used for downstream analysis and visualization in MapMan 3.6 (Lohse et al., 2014; Thimm et al., 2004).

Citrate synthase activity

Protein extraction was carried out in BEB followed by desalting with PD-10 columns (GE Healthcare, Solingen, Germany). The protein extract was treated with deacetylase inhibitors (3 μM apicidin [Darkin-Rattray et al., 1996] and 1 mM nicotinamide [Schmidt et al., 2004]). Citrate synthase activity was measured spectrophotometrically as described previously (Schmidtmann et al., 2014). The assay was based on the absorbance of DTNB after reaction with CoA at 412 nm. Prepared protein extract (100 μg) was incubated with 0.5 mM acetyl-CoA (AppliChem, Darmsatdt, Germany) in 1 mM DTNB (in 100 mM Tris–HCl pH 8.0) and the reaction was started after addition of 10 mM oxaloacetate.

Experimental design and statistical rationale

To work with the same starting material, a pre-culture of *Chlamydomonas* cells was split into three sub-cultures per condition (heterotroph, mixotroph, photoautotroph). Samples were randomly numbered 1–3 and every first, second, or third replicate sample from each condition was selected for differential dimethyl labeling to end with a light, medium, and heavy dimethyl-labeled peptide sample, which were pooled for subsequent MS analysis. The light, medium, and heavy isotopes were swapped in the third replicate to prevent any labeling bias in the data analysis. Statistical tests used to analyze data are indicated in the respective figure legends.

ACKNOWLEDGMENTS

This work was supported by the Max-Planck Society and the University of Muenster. Open Access funding enabled and organized by Projekt DEAL.

AUTHOR CONTRIBUTIONS

MF, A-CK, MH, LK, AH, A-VB, and KK performed research; A-CK, MH, A-VB, JN, and IF designed research; A-CK, MF,

MH, KK, and JE analyzed data; MF, A-CK, JE, DL, and IF wrote the paper.

CONFLICTS OF INTEREST

The authors declare that they have no conflict of interest.

DATA AVAILABILITY STATEMENT

The raw MS data and MaxQuant output files have been deposited to the ProteomeXchange Consortium (http://proteomecentral.proteomexchange.org) via the JPOST partner repository (Vizcaino et al., 2014) with the dataset identifiers PXD025168 and JPST001115.

SUPPORTING INFORMATION

Additional Supporting Information may be found in the online version of this article.

Figure S1. Stitch DB network of proteins associated with acetate.

Figure S2. Stitch DB network of proteins associated with carbon dioxide.

Figure S3. Protein sequence alignments.

Table S1. Quantitative proteome analysis.

Table S2. Quantitative acetylome data analysis.

Table S3. Acetylation site occupancies.

Table S4. AcK fold changes of proteins involved in fatty acid metabolism.

REFERENCES

Atteia, A., Adrait, A., Brugiere, S., Tardif, M., van Lis, R., Deusch, O. *et al.* (2009) A proteomic survey of Chlamydomonas reinhardtii mitochondria sheds new light on the metabolic plasticity of the organelle and on the nature of the alpha-proteobacterial mitochondrial ancestor. *Molecular Biology and Evolution*, **26**, 1533–1548.

Baeza, J., Dowell, J.A., Smallegan, M.J., Fan, J., Amador-Noguez, D., Khan, Z. *et al.* (2014) Stoichiometry of site-specific lysine acetylation in an entire proteome. *Journal of Biological Chemistry*, **289**, 21326–21338.

Balparda, M., Elsässer, M., Badia, M. B., Giese, J., Bovdilova, A. & Hüdig, M., *et al.* (2021) Acetylation of conserved lysines fine-tunes mitochondrial malate dehydrogenase activity in land plants. *The Plant Journal*. https://doi.org/10.1111/tpj.15556

Bogaert, K.A., Perez, E., Rumin, J., Giltay, A., Carone, M., Coosemans, N. *et al.* (2019) Metabolic, physiological, and transcriptomics analysis of batch cultures of the green microalga Chlamydomonas grown on different acetate concentrations. *Cells*, **8**, 1367.

Bohne, A.V., Schwarz, C., Schottkowski, M., Lidschreiber, M., Piotrowski, M., Zerges, W. *et al.* (2013) Reciprocal regulation of protein synthesis and carbon metabolism for thylakoid membrane biogenesis. *PLoS Biology*, **11**, e1001482.

Boyle, N.R. & Morgan, J.A. (2009) Flux balance analysis of primary metabolism in Chlamydomonas reinhardtii. *BMC Systems Biology*, **3**, 4.

Boyle, N.R., Sengupta, N. & Morgan, J.A. (2017) Metabolic flux analysis of heterotrophic growth in Chlamydomonas reinhardtii. *PLoS One*, **12**, e0177292.

Castano-Cerezo, S., Bernal, V., Post, H., Fuhrer, T., Cappadona, S., Sanchez-Diaz, N.C. *et al.* (2014) Protein acetylation affects acetate metabolism, motility and acid stress response in Escherichia coli. *Molecular Systems Biology*, **10**, 762.

Choudhary, C., Weinert, B.T., Nishida, Y., Verdin, E. & Mann, M. (2014) The growing landscape of lysine acetylation links metabolism and cell signalling. *Nature Reviews Molecular Cell Biology*, **15**, 536–550.

Cobbold, S.A., Santos, J.M., Ochoa, A., Perlman, D.H. & Llinas, M. (2016) Proteome-wide analysis reveals widespread lysine acetylation of major protein complexes in the malaria parasite. *Scientific Reports*, **6**, 19722.

Colaert, N., Helsens, K., Martens, L., Vandekerckhove, J. & Gevaert, K. (2009) Improved visualization of protein consensus sequences by iceLogo. *Nature Methods*, **6**, 786–787.

Cox, J., Hein, M.Y., Luber, C.A., Paron, I., Nagaraj, N. & Mann, M. (2014) Accurate proteome-wide label-free quantification by delayed normalization and maximal peptide ratio extraction, termed MaxLFQ. *Molecular & Cellular Proteomics*, **13**, 2513–2526.

Cox, J. & Mann, M. (2008) MaxQuant enables high peptide identification rates, individualized p.p.b.-range mass accuracies and proteome-wide protein quantification. *Nature Biotechnology*, **26**, 1367–1372.

Crosby, H.A., Heiniger, E.K., Harwood, C.S. & Escalante-Semerena, J.C. (2010) Reversible N epsilon-lysine acetylation regulates the activity of acyl-CoA synthetases involved in anaerobic benzoate catabolism in Rhodopseudomonas palustris. *Molecular Microbiology*, **76**, 874–888.

Darkin-Rattray, S.J., Gurnett, A.M., Myers, R.W., Dulski, P.M., Crumley, T.M., Allocco, J.J. *et al.* (1996) Apicidin: a novel antiprotozoal agent that inhibits parasite histone deacetylase. *Proceedings of the National Academy of Sciences of the United States of America*, **93**, 13143–13147.

Durante, L., Hubner, W., Lauersen, K.J. & Remacle, C. (2019) Characterization of the GPR1/FUN34/YaaH protein family in the green microalga Chlamydomonas suggests their role as intracellular membrane acetate channels. *Plant Direct*, **3**, e00148.

Erickson, E., Wakao, S. & Niyogi, K.K. (2015) Light stress and photoprotection in Chlamydomonas reinhardtii. *The Plant Journal*, **82**, 449–465.

Fang, X., Chen, W., Zhao, Y., Ruan, S., Zhang, H., Yan, C. *et al.* (2015) Global analysis of lysine acetylation in strawberry leaves. *Frontiers in Plant Science*, **6**, 739.

Fernandes, J., Weddle, A., Kinter, C.S., Humphries, K.M., Mather, T., Szweda, L.I. *et al.* (2015) Lysine Acetylation Activates Mitochondrial Aconitase in the Heart. *Biochemistry*, **54**, 4008–4018.

Finkemeier, I., Laxa, M., Miguet, L., Howden, A.J. & Sweetlove, L.J. (2011) Proteins of diverse function and subcellular location are lysine acetylated in Arabidopsis. *Plant Physiology*, **155**, 1779–1790.

Gao, X., Hong, H., Li, W.C., Yang, L., Huang, J., Xiao, Y.L. *et al.* (2016) Downregulation of rubisco activity by non-enzymatic acetylation of RbcL. *Molecular Plant*, **9**, 1018–1027.

Gardner, J.G., Grundy, F.J., Henkin, T.M. & Escalante-Semerena, J.C. (2006) Control of acetyl-coenzyme A synthetase (AcsA) activity by acetylation/deacetylation without NAD(+) involvement in Bacillus subtilis. *Journal of Bacteriology*, **188**, 5460–5468.

Giese, J., Lassowskat, I. & Finkemeier, I. (2020) High-resolution lysine acetylome profiling by offline fractionation and immunoprecipitation. *Methods in Molecular Biology*, **2139**, 241–256.

Goodenough, U., Blaby, I., Casero, D., Gallaher, S.D., Goodson, C., Johnson, S. *et al.* (2014) The path to triacylglyceride obesity in the sta6 strain of Chlamydomonas reinhardtii. *Eukaryotic Cell*, **13**, 591–613.

Goodstein, D.M., Shu, S., Howson, R., Neupane, R., Hayes, R.D., Fazo, J. *et al.* (2012) Phytozome: a comparative platform for green plant genomics. *Nucleic Acids Research*, **40**, D1178–1186.

Gorman, D.S. & Levine, R.P. (1965) Cytochrome f and plastocyanin: their sequence in the photosynthetic electron transport chain of Chlamydomonas reinhardi. *Proceedings of the National Academy of Sciences of the United States of America*, **54**, 1665–1669.

Graves, L.B. Jr, Hanzely, L. & Trelease, R.N. (1971) The occurrence and fine structural characterization of microbodies in Euglena gracilis. *Protoplasma*, **72**, 141–152.

Hallmann, A. (2011) Evolution of reproductive development in the volvocine algae. *Sexual Plant Reproduction*, **24**, 97–112.

Hansen, B.K., Gupta, R., Baldus, L., Lyon, D., Narita, T., Lammers, M. *et al.* (2019) Analysis of human acetylation stoichiometry defines mechanistic constraints on protein regulation. *Nature Communications*, **10**, 1055.

Harris, E.H. (1989) 2 - Culture and Storage Methods. In: Harris, E.H. (Ed.) *The Chlamydomonas sourcebook*. Academic Press, pp. 25–63. Available at: https://www.sciencedirect.com/science/article/pii/B9780123268808500079

Hartl, M., Füssl, M., Boersema, P.J., Jost, J.O., Kramer, K., Bakirbas, A. *et al.* (2017) Lysine acetylome profiling uncovers novel histone deacetylase substrate proteins in Arabidopsis. *Molecular Systems Biology*, **13**, 949.

Hartl, M., König, A.C. & Finkemeier, I. (2015) Identification of lysine-acetylated mitochondrial proteins and their acetylation sites. *Methods in Molecular Biology*, **1305**, 107–121.

Hayashi, Y., Sato, N., Shinozaki, A. & Watanabe, M. (2015) Increase in peroxisome number and the gene expression of putative glyoxysomal enzymes in Chlamydomonas cells supplemented with acetate. *Journal of Plant Research*, **128**, 177–185.

Henriksen, P., Wagner, S.A., Weinert, B.T., Sharma, S., Bacinskaja, G., Rehman, M. *et al.* (2012) Proteome-wide analysis of lysine acetylation suggests its broad regulatory scope in Saccharomyces cerevisiae. *Molecular & Cellular Proteomics*, **11**, 1510–1522.

Hoober, J.K. (1989) The Chlamydomonas Sourcebook. A Comprehensive Guide to Biology and Laboratory Use. Elizabeth H. Harris. Academic Press, San Diego, CA, 1989. xiv, 780 pp., illus. $145. *Science*, **246**, 1503–1504.

Hosp, F., Lassowskat, I., Santoro, V., De Vleesschauwer, D., Fliegner, D., Redestig, H. *et al.* (2017) Lysine acetylation in mitochondria: from inventory to function. *Mitochondrion*, **33**, 58–71.

Jing, E., O'Neill, B.T., Rardin, M.J., Kleinridders, A., Ilkeyeva, O.R., Ussar, S. *et al.* (2013) Sirt3 regulates metabolic flexibility of skeletal muscle through reversible enzymatic deacetylation. *Diabetes*, **62**, 3404–3417.

Kato, J., Yamahara, T., Tanaka, K., Takio, S. & Satoh, T. (1997) Characterization of catalase from green algae Chlamydomonas reinhardtii. *Journal of Plant Physiology*, **151**, 262–268.

Kaur, S., Hérault, J., Caruso, A., Pencréac'h, G., Come, M., Gauvry, L. *et al.* (2021) Proteomics and expression studies on lipids and fatty acids metabolic genes in Isochrysis galbana under the combined influence of nitrogen starvation and sodium acetate supplementation. *Bioresource Technology Reports*, **15**, 100714.

Knight, S., Andersson, I. & Brändén, C.-I. (1990) Crystallographic analysis of ribulose 1,5-bisphosphate carboxylase from spinach at 2·4 Å resolution: subunit interactions and active site. *Journal of Molecular Biology*, **215**, 113–160.

König, A.-C., Hartl, M., Boersema, P.J., Mann, M. & Finkemeier, I. (2014) The mitochondrial lysine acetylome of Arabidopsis. *Mitochondrion*, **19**, 252–260.

Koskela, M.M., Brünje, A., Ivanauskaite, A., Lopez, L.S., Schneider, D., DeTar, R.A. *et al.* (2020) Comparative analysis of thylakoid protein complexes in state transition mutants nsi and stn7: focus on PSI and LHCII. *Photosynthesis Research*, **145**, 15–30.

Kunze, M., Pracharoenwattana, I., Smith, S.M. & Hartig, A. (2006) A central role for the peroxisomal membrane in glyoxylate cycle function. *Biochimica Et Biophysica Acta (BBA) - Molecular Cell Research*, **1763**, 1441–1452.

Lassowskat, I., Hartl, M., Hosp, F., Boersema, P.J., Mann, M. & Finkemeier, I. (2017) Dimethyl-labeling-based quantification of the lysine acetylome and proteome of plants. In: Fernie, A.R., Bauwe, H. & Weber, A.P.M. (Eds.) *Photorespiration*. New York, NY: Springer New York, pp. 65–81

Lauersen, K.J., Willamme, R., Coosemans, N., Joris, M., Kruse, O. & Remacle, C. (2016) Peroxisomal microbodies are at the crossroads of acetate assimilation in the green microalga Chlamydomonas reinhardtii. *Algal Research*, **16**, 266–274. https://doi.org/10.1016/j.algal.2016.03.026

Ledford, H.K., Chin, B.L. & Niyogi, K.K. (2007) Acclimation to singlet oxygen stress in Chlamydomonas reinhardtii. *Eukaryotic Cell*, **6**, 919–930.

Leite, G.B., Abdelaziz, A.E. & Hallenbeck, P.C. (2013) Algal biofuels: challenges and opportunities. *Bioresource Technology*, **145**, 134–141.

L'Hernault, S.W. & Rosenbaum, J.L. (1983) Chlamydomonas alpha-tubulin is posttranslationally modified in the flagella during flagellar assembly. *Journal of Cell Biology*, **97**, 258–263.

L'Hernault, S.W. & Rosenbaum, J.L. (1985) Chlamydomonas alpha-tubulin is posttranslationally modified by acetylation on the epsilon-amino group of a lysine. *Biochemistry*, **24**, 473–478.

Lingard, M.J. & Trelease, R.N. (2006) Five Arabidopsis peroxin 11 homologs individually promote peroxisome elongation, duplication or aggregation. *Journal of Cell Science*, **119**, 1961–1972.

Liu, F., Yang, M., Wang, X., Yang, S., Gu, J., Zhou, J. *et al.* (2014) Acetylome analysis reveals diverse functions of lysine acetylation in Mycobacterium tuberculosis. *Molecular & Cellular Proteomics*, **13**, 3352–3366.

Liu, Z., Song, J., Miao, W., Yang, B., Zhang, Z., Chen, W. *et al.* (2021) Comprehensive proteome and lysine acetylome analysis reveals the widespread involvement of acetylation in cold resistance of pepper (Capsicum annuum L.). *Frontiers in Plant Science*, **12**, 730489.

Lohse, M., Nagel, A., Herter, T., May, P., Schroda, M., Zrenner, R. *et al.* (2014) Mercator: a fast and simple web server for genome scale functional annotation of plant sequence data. *Plant, Cell and Environment*, **37**, 1250–1258.

Magneschi, L., Catalanotti, C., Subramanian, V., Dubini, A., Yang, W., Mus, F. *et al.* (2012) A mutant in the ADH1 gene of Chlamydomonas reinhardtii elicits metabolic restructuring during anaerobiosis. *Plant Physiology*, **158**, 1293–1305.

Merchant, S.S., Kropat, J., Liu, B.S., Shaw, J. & Warakanont, J. (2012) TAG, You're it! Chlamydomonas as a reference organism for understanding algal triacylglycerol accumulation. *Current Opinion in Biotechnology*, **23**, 352–363.

Merchant, S.S., Prochnik, S.E., Vallon, O., Harris, E.H., Karpowicz, S.J., Witman, G.B. *et al.* (2007) The Chlamydomonas genome reveals the evolution of key animal and plant functions. *Science*, **318**, 245–250.

Nakayasu, E.S., Wu, S., Sydor, M.A., Shukla, A.K., Weitz, K.K., Moore, R.J. *et al.* (2014) A method to determine lysine acetylation stoichiometries. *International Journal of Proteomics*, **2014**, 730725.

Narita, T., Weinert, B.T. & Choudhary C. (2019) Functions and mechanisms of non-histone protein acetylation. *Nature Reviews Molecular Cell Biology*, **20**, 156–174.

Olsen, J.V., Vermeulen, M., Santamaria, A., Kumar, C., Miller, M.L., Jensen, L.J. *et al.* (2010) Quantitative phosphoproteomics reveals widespread full phosphorylation site occupancy during mitosis. *Science Signalling*, **3**, ra3.

Plancke, C., Vigeolas, H., Hohner, R., Roberty, S., Emonds-Alt, B., Larosa, V. *et al.* (2014) Lack of isocitrate lyase in Chlamydomonas leads to changes in carbon metabolism and in the response to oxidative stress under mixotrophic growth. *The Plant Journal*, **77**, 404–417.

R Core Team. (2016) *R: A language and environment for statistical computing*. Vienna: R Foundation for Statistical Computing. Available at: https://www.R-project.org/

Rai, M.P., Nigam, S. & Sharma, R. (2013) Response of growth and fatty acid compositions of Chlorella pyrenoidosa under mixotrophic cultivation with acetate and glycerol for bioenergy application. *Biomass and Bioenergy*, **58**, 251–257.

Ritchie, M.E., Phipson, B., Wu, D., Hu, Y., Law, C.W., Shi, W. *et al.* (2015) Limma powers differential expression analyses for RNA-sequencing and microarray studies. *Nucleic Acids Research*, **43**, e47.

Roach, T., Sedoud, A. & Krieger-Liszkay, A. (2013) Acetate in mixotrophic growth medium affects photosystem II in Chlamydomonas reinhardtii and protects against photoinhibition. *Biochimica Et Biophysica Acta*, **1827**, 1183–1190.

Sager, R. & Granick, S. (1953) Nutritional studies with Chlamydomonas reinhardi. *Annals of the New York Academy of Sciences*, **56**, 831–838.

Schilling, B., Christensen, D., Davis, R., Sahu, A.K., Hu, L.I., Walker-Peddakotla, A. *et al.* (2015) Protein acetylation dynamics in response to carbon overflow in Escherichia coli. *Molecular Microbiology*, **98**, 847–863.

Schmidt, C., Beilsten-Edmands, V., Mohammed, S. & Robinson, C.V. (2017) Acetylation and phosphorylation control both local and global stability of the chloroplast F1 ATP synthase. *Scientific Reports*, **7**, 44068.

Schmidt, M.T., Smith, B.C., Jackson, M.D. & Denu, J.M. (2004) Coenzyme specificity of Sir2 protein deacetylases: implications for physiological regulation. *Journal of Biological Chemistry*, **279**, 40122–40129.

Schmidtmann, E., König, A.C., Orwat, A., Leister, D., Hartl, M. & Finkemeier, I. (2014) Redox regulation of arabidopsis mitochondrial citrate synthase. *Molecular Plant*, **7**, 156–169.

Schwacke, R., Ponce-Soto, G.Y., Krause, K., Bolger, A.M., Arsova, B., Hallab, A. *et al.* (2019) MapMan4: a refined protein classification and annotation framework applicable to multi-omics data analysis. *Molecular Plant*, **12**, 879–892.

Scranton, M.A., Ostrand, J.T., Fields, F.J. & Mayfield, S.P. (2015) Chlamydomonas as a model for biofuels and bio-products production. *The Plant Journal*, **82**, 523–531.

Shannon, P., Markiel, A., Ozier, O., Baliga, N.S., Wang, J.T., Ramage, D. *et al.* (2003) Cytoscape: a software environment for integrated models of biomolecular interaction networks. *Genome Research*, **13**, 2498–2504.

Smith, R.T., Bangert, K., Wilkinson, S.J. & Gilmour, D.J. (2015) Synergistic carbon metabolism in a fast growing mixotrophic freshwater microalgal species Micractinium inermum. *Biomass and Bioenergy*, **82**, 73–86.

Stabenau, H. (1974) Localization of enzymes of glycolate metabolism in the alga chlorogonium elongatum. *Plant Physiology*, **54**, 921–924.

Stabenau, H., Winkler, U. & Säftel, W. (1993) Localization of glycolate dehydrogenase in two species of Dunaliella. *Planta*, **191**, 362–364.

Starai, V.J., Celic, I., Cole, R.N., Boeke, J.D. & Escalante-Semerena, J.C. (2002) Sir2-dependent activation of acetyl-CoA synthetase by deacetylation of active lysine. *Science*, **298**, 2390–2392.

Starai, V.J. & Escalante-Semerena, J.C. (2004) Identification of the protein acetyltransferase (Pat) enzyme that acetylates acetyl-CoA synthetase in Salmonella enterica. *Journal of Molecular Biology*, **340**, 1005–1012.

Sterner, D.E. & Berger, S.L. (2000) Acetylation of histones and transcription-related factors. *Microbiology and Molecular Biology Reviews*, **64**, 435–459.

Szklarczyk, D., Santos, A., von Mering, C., Jensen, L.J., Bork, P. & Kuhn, M. (2016) STITCH 5: augmenting protein-chemical interaction networks with tissue and affinity data. *Nucleic Acids Research*, **44**, D380–D384.

Thimm, O., Blasing, O., Gibon, Y., Nagel, A., Meyer, S., Kruger, P. *et al.* (2004) MAPMAN: a user-driven tool to display genomics data sets onto diagrams of metabolic pathways and other biological processes. *The Plant Journal*, **37**, 914–939.

Tirumani, S., Kokkanti, M., Chaudhari, V., Shukla, M. & Rao, B.J. (2014) Regulation of CCM genes in Chlamydomonas reinhardtii during conditions of light-dark cycles in synchronous cultures. *Plant Molecular Biology*, **85**, 277–286.

Tyanova, S., Temu, T. & Cox, J. (2016) The MaxQuant computational platform for mass spectrometry-based shotgun proteomics. *Nature Protocols*, **11**, 2301–2319.

Uhrig, R.G., Schlapfer, P., Roschitzki, B., Hirsch-Hoffmann, M. & Gruissem, W. (2019) Diurnal changes in concerted plant protein phosphorylation and acetylation in Arabidopsis organs and seedlings. *The Plant Journal*, **99**, 176–194.

Vizcaino, J.A., Deutsch, E.W., Wang, R., Csordas, A., Reisinger, F., Rios, D. *et al.* (2014) ProteomeXchange provides globally coordinated proteomics data submission and dissemination. *Nature Biotechnology*, **32**, 223–226.

Wagner, G.R. & Payne, R.M. (2013) Widespread and enzyme-independent Nepsilon-acetylation and Nepsilon-succinylation of proteins in the chemical conditions of the mitochondrial matrix. *Journal of Biological Chemistry*, **288**, 29036–29045.

Wang, Q., Zhang, Y., Yang, C., Xiong, H., Lin, Y., Yao, J. *et al.* (2010) Acetylation of metabolic enzymes coordinates carbon source utilization and metabolic flux. *Science*, **327**, 1004–1007.

Weinert, B.T., Satpathy, S., Hansen, B.K., Lyon, D., Jensen, L.J. & Choudhary, C. (2017) Accurate quantification of site-specific acetylation stoichiometry reveals the impact of sirtuin deacetylase CobB on the E. coli acetylome. *Molecular & Cellular Proteomics*, **16**, 759–769.

Wisniewski, J.R., Zougman, A., Nagaraj, N. & Mann, M. (2009) Universal sample preparation method for proteome analysis. *Nature Methods*, **6**, 359–362.

Work, V.H., Radakovits, R., Jinkerson, R.E., Meuser, J.E., Elliott, L.G., Vinyard, D.J. *et al.* (2010) Increased lipid accumulation in the Chlamydomonas reinhardtii sta7-10 starchless isoamylase mutant and increased carbohydrate synthesis in complemented strains. *Eukaryotic Cell*, **9**, 1251–1261.

Wu, X., Oh, M.H., Schwarz, E.M., Larue, C.T., Sivaguru, M., Imai, B.S. *et al.* (2011) Lysine acetylation is a widespread protein modification for diverse proteins in Arabidopsis. *Plant Physiology*, **155**, 1769–1778.

Xue, H., Tokutsu, R., Bergner, S.V., Scholz, M., Minagawa, J. & Hippler, M. (2015) PHOTOSYSTEM II SUBUNIT R is required for efficient binding of LIGHT-HARVESTING COMPLEX STRESS-RELATED PROTEIN3 to photosystem II-light-harvesting supercomplexes in Chlamydomonas reinhardtii. *Plant Physiology*, **167**, 1566–1578.

Yang, W., Catalanotti, C., D'Adamo, S., Wittkopp, T.M., Ingram-Smith, C.J., Mackinder, L. *et al.* (2014) Alternative acetate production pathways in Chlamydomonas reinhardtii during dark anoxia and the dominant role of chloroplasts in fermentative acetate production. *The Plant Cell*, **26**, 4499–4518.

Ynalvez, R.A., Xiao, Y., Ward, A.S., Cunnusamy, K. & Moroney, J.V. (2008) Identification and characterization of two closely related beta-carbonic anhydrases from Chlamydomonas reinhardtii. *Physiologia Plantarum*, **133**, 15–26.

Zhao, S., Xu, W., Jiang, W., Yu, W., Lin, Y., Zhang, T. *et al.* (2010) Regulation of cellular metabolism by protein lysine acetylation. *Science*, **327**, 1000–1004.

Zhou, H., Finkemeier, I., Guan, W., Tossounian, M.A., Wei, B., Young, D. *et al.* (2018) Oxidative stress-triggered interactions between the succinyl- and acetyl-proteomes of rice leaves. *Plant, Cell and Environment*, **41**, 1139–1153.